Geotechnical Engineering Journal of the SEAGS & AGSSEA Vol. 42 No.4 December 2011 ISSN 0046-5828

Simulating Shear Rate-dependent Undrained Stress-Strain Behaviour Of Natural Sedimentary Clayat Kobe Airport

MinSu Jung[1] and Satoru Shibuya[2]
[1]*Geotechnical Engineering Research Division, Korea Institute of Construction Technology, Ilsan, Korea*
[2] *Graduate School of Civil Engineering, Kobe University, Kobe, Japan*
E-mail: msung@kict.re.kr

ABSTRACT: Effects of strain rate on undrained shear behaviour of seabed Holocene clay at Kobe airport site were examined in a series of triaxial compression and extension tests performed using different rate of axial straining. A comparative compression test in which the strain rate was changed in steps was also carried out. Similar tests were performed in constant-volume direct shear box (DSB) test. It was found that the undrained strength increased with increasing shear rate and increasing consolidation period. Isotach properties seemed a key to govern the undrained shear behaviour. The behaviour can be described such that the stress-strain response as well as the development of excess pore pressures was uniquely related to the axial strain rate, for which softer and more contracting response was examined when the rate of axial strain decreased, and vice versa as the axial strain rate increased. In this paper, a type of Isotach stress-strain response of the clay, together with the development of drained creep strain with time was successfully simulated by newly developed models.

1. INTRODUCTION

Strain rate effects are significant for undrained shear behaviour of clay (for example, Bjerrum, 1972, Vaid et al, 1977, Graham et al, 1983, Oshima et al, 1991, Di Benedetto et al, 1997). The undrained shear strength, for instance, increases with the strain rate and also with the sustained consolidation period prior to undrained shear. Moreover, the stress-strain behaviour of a wide spectrum of geomaterials may be characterized with Isotach properties (see, Tatsuoka et al, 1999). In engineering practices, it is thus important to take account of such rate effects when applying the undrained strength from laboratory tests to in-situ problems such as the embankment on soft ground. It is widely recognized that the strain rate is a prevailing factor to govern the stress-strain and strength response of clay when subjected to undrained shearing (Hanzawa et al, 1981). The concept of Isotach properties of soil (Šuklie, 1969) is then useful for describing such rate effects by postulating that the current stress is uniquely related to the current irrecoverable strain as well as the strain rate (for example, see Tatsuoka et al, 1999, Di Benedetto et al, 2002).

In this paper, the shear rate effects of Holocene clay from Kobe airport site (see Fujiwara et al, 2008) were thoroughly examined in the laboratory. Also, the stress-strain relationship from the pseudo-elastic region involved with the order of strains of 0.001% to the post-peak up to axial strain of 15% was successfully simulated by an Isotach model. The development of creep strain with time under constant vertical stress was also simulated by the model.

2. MOTHODOLOGY

Figure 1 shows the triaxial apparatus (for details, see Shibuya et al, 2001). In this apparatus, the specimen having the size of 50mm in diameter and 100mm in height is subjected to consolidation and shear in a fully automated manner. Figure 2 shows the DSB apparatus developed at Kobe University. Like the triaxial apparatus, the vertical as well as the horizontal displacement of the disk-shaped specimen with 60mm in diameter and 40mm in height can each be controlled by using a digital servo-motor (Shibuya et al., 2005).

Constant-volume conditions can be readily achieved by maintaining the vertical movement zero during the shear. The vertical load is measured at the bottom of the lower shear box, implying that the vertical stress is free from any frictions between the soil specimen and the shear box wall (refer to Shibuya et al, 1997). In all the tests performed in this study, the clearance between the upper and lower shear boxes was maintained constant at 0.2mm.

The clay samples were retrieved from Holocene deposit underneath Kobe airport (Fujiwara et al, 2008) by using a fixed-piston thin-wall sampler.

The fully saturated natural specimens were each consolidated to the prescribed stress, and it was sheared under undrained conditions in triaxial test and constant-volume (i.e., undrained) conditions in DSB test, respectively.

Tables 1 and 2 show the details of the triaxial and DSB tests performed, respectively. It should be mentioned that the end of primary consolidation was judged based on the 3t-method (JGS, 1979). However, in some tests, the consolidation period was longer than the standard in order to examine the effects of consolidation period.

3. TEST RESULTS

Figures 3 and 4 show the variation of void ratio, *e*, with time during consolidation as examined in triaxial and DSB tests, respectively. The stress-strain relationship of a series of triaxial tests using the axial strain rate of 0.02 %/min is shown in Figure 5. The undrained effective stress paths are shown in Figure 6 in which the deviator stress, *q*, is plotted against the mean effective stress, *p'*.

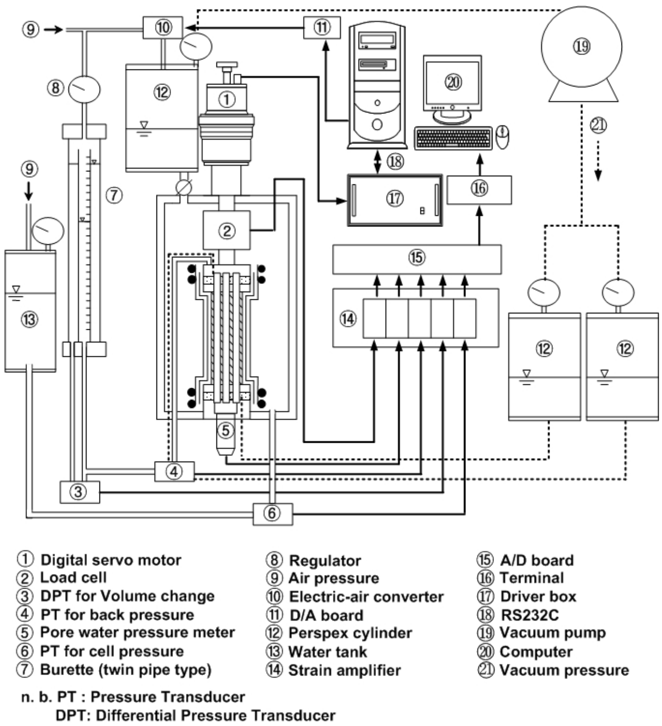

Figure 1 Triaxial apparatus employed.

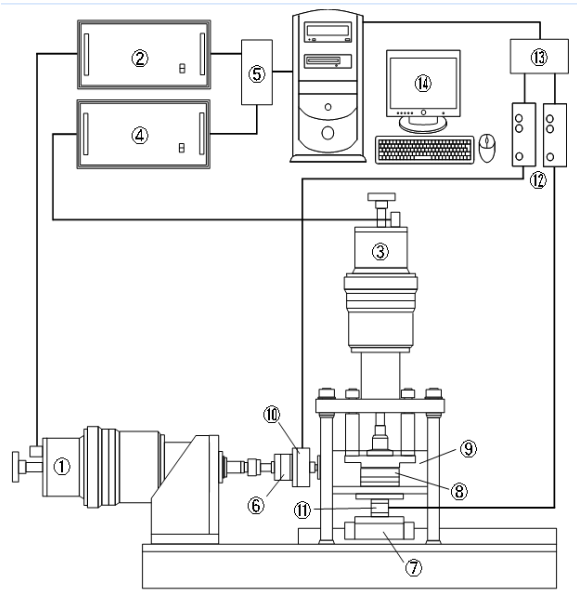

①:direct drive motor for lateral loading ②:drive init for lateral loading ③:direct drive motor for vertical loading ④:drive unit for vertical loading ⑤:serial correspondence board ⑥:slide unit ⑦:linear roller way ⑧:shear box ⑨:outer box ⑩:load cell for lateral loading ⑪:load cell for vertical loading ⑫:strain amplifier ⑬:AD transformation board ⑭:personal computer

Figure 2 Direct shear box apparatus employed.

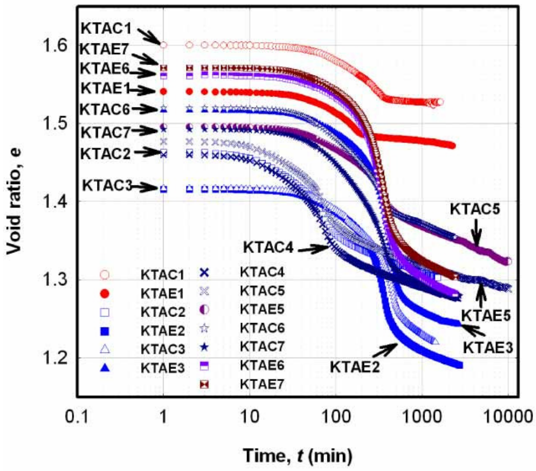

(a) anisotropically consolidated specimens

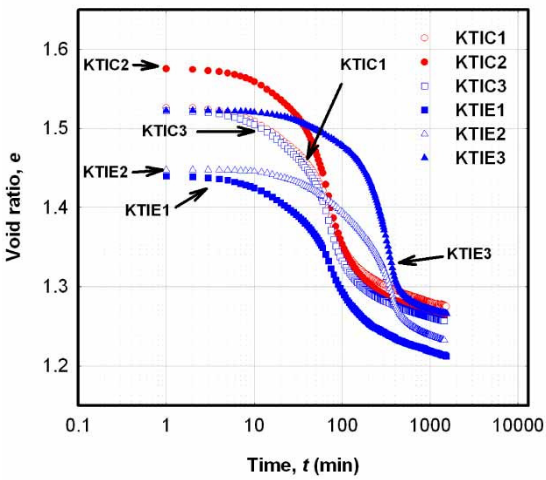

(b) isotropically consolidated specimens

Figure 3 Variation of void ratio, e, with time during consolidation as examined in triaxial tests.

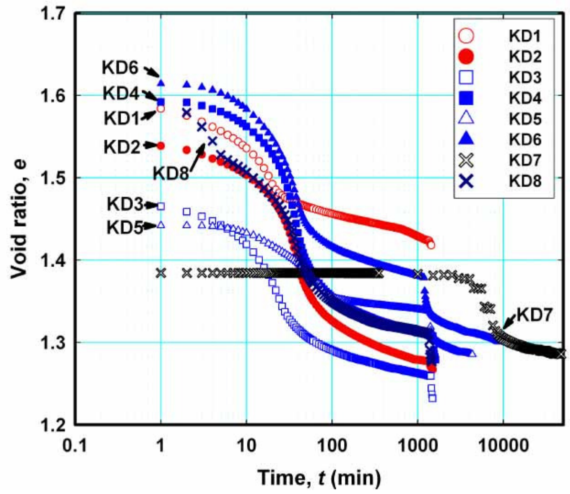

Figure 4 Variation of void ratio, e, with time during consolidation as examined in DSB tests.

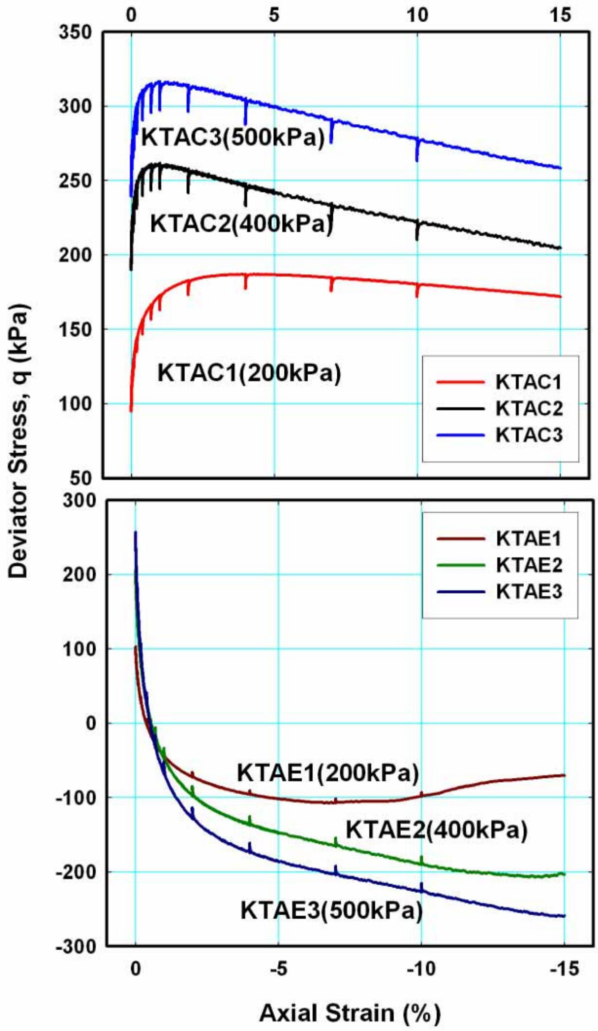

Figure 5 Stress-strain relationship of a series of triaxial tests using the axial strain rate of 0.02 %/min

The results of the constant-volume DSB tests are shown in Figure7, in which the variation of the horizontal shear stress, τ, is plotted against horizontal displacement and the vertical stress. Despite that the specimens were all normally consolidated, the stress-strain relationship exhibited softening behaviour when sheared undrained.

Table 1 Conditions of undrained triaxial test.

ID	K.P (-m)	γ_t (kN/m3)	σ_{v0} (kPa)	Initial water content (%)	Consolidation conditions		Shearing rate (%/min)	Creep-strain-rate $\Delta\varepsilon_v$ ($\times 10^4$ %/min)	B value
					σ'_{v0} (kPa)	Consolidation time (min)			
KTAC1	23.5	16.04	180	55.8	200	1629(3.1t)	0.02	1.683	0.95
KTAE1	25.5	15.50	163	55.9		2264(9.7t)		2.385	0.96
KTAC2	32.5	16.60	162	53.5	400	1520(11.4t)		7.070	0.95
KTAE2	26.5	17.17	172	57.5		2732(7.5t)		2.018	0.96
KTAE3	25.5	16.11	163	53.8		2662(4.4t)		1.951	0.97
KTAC4	34.5	16.29	175	54.1	400 (An-isotro-pically)	2620(15.7t)		2.600	0.98
KTAC5	34.5	16.29	175	53.3		10122(58.4t)		1.494	0.95
KTAE5	35.5	16.37	181	54.9		10082(18.9t)		3.528	0.95
KTAC6	38.5	16.02	198	55.5		2406(4.8t)	0.1	2.283	0.97
KTAC7	39.5	16.15	198	56.5		2702(5.4t)	1	3.333	0.95
KTAE6	24.5	16.42	182	59.2		2408(4.8t)	0.1	2.657	0.96
KTAE7	24.5	16.37	182	59.6		2439(4.9t)	1	3.403	0.97
KTIC1	33.5	16.21	168	55.7	400 (isotro-pically)	1520(7.6t)	0.02	1.326	0.95
KTIC2	26.5	16.04	167	56.6		1455(7.3t)	0.1	4.411	0.97
KTIC3	27.3	16.21	171	51.3		1453(8.7t)	1	3.442	0.95
KTIE1	33.5	16.39	168	52.3		1522(4.6t)	0.02	8.127	0.95
KTIE2	28.5	16.29	175	53.0		1443(3.3t)	0.1	5.268	0.96
KTIE3	28.5	16.09	175	53.9		1545(3.1t)	1	3.376	0.95

Table 2 Conditions of constant-volume direct shear box tests.

ID	K.P (-m)	γ_t (kN/m^3)	σ_{v0} (kPa)	Initial water content (%)	Consolidation condition		Shear speed (mm/min)
					σ'_{v0} (kPa)	Consolidation time (min)	
KD1	28.5	15.89	174	55.0	200	1433(61t)	0.1
KD2	26.5	16.18	172	55.7	400	1486(23t)	
KD3	28.5	16.33	174	52.6	500	1483(32t)	
KD4	24.5	16.02	182	57.4	400	1606(27t)	0.02
KD5	29.5	16.05	172	55.4		4321(72t)	
KD6	29.5	15.83	172	56.8		10083(151t)	
KD7	29.3	16.64	174	48.0		39894(198t)	
KD8	25.5	15.92	163	55.6		1457(22t)	1

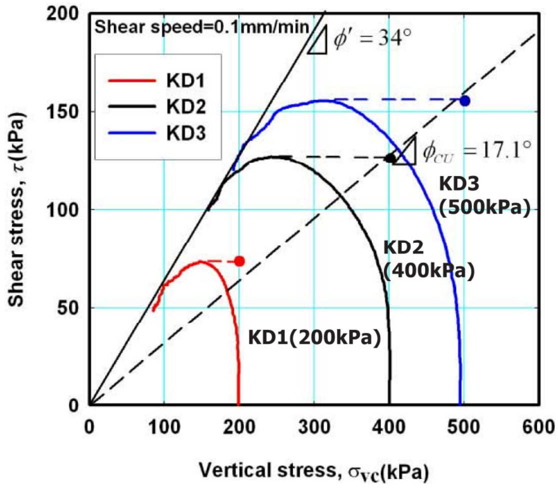

(a) τ-σ_{vc} relationship

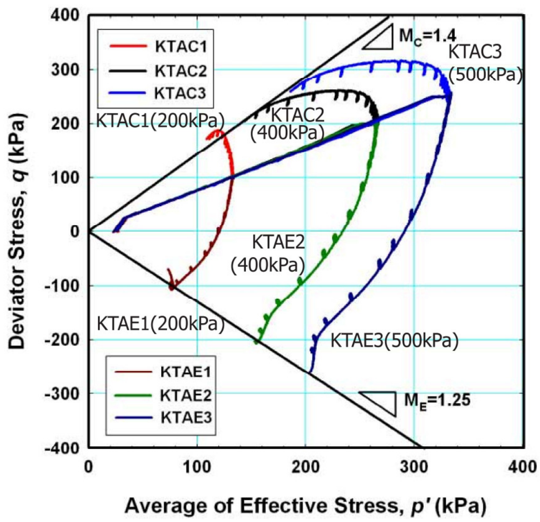

Figure 6 Undrained effective stress paths of a series of triaxial tests using the axial strain rate of 0.02 %/min

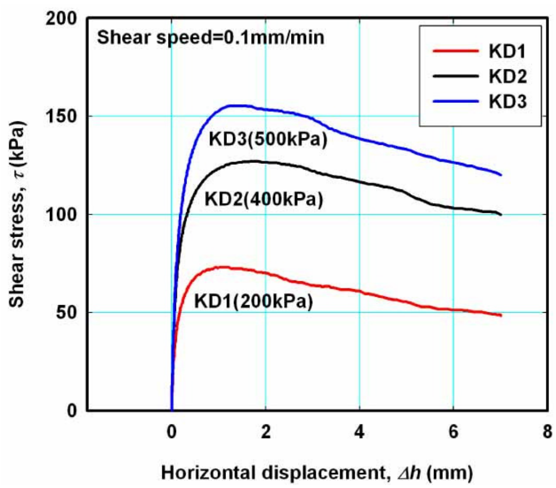

(b) τ-Δh relationship

Figure 7 Results of constant-volume DSB tests with the horizontal displacement rate of 0.1mm/min.

4. COMPARISONS AND DISCUSSIONS

4.1 Effects of consolidation period

Figures 8 and 9 show the results of triaxial tests performed using different consolidation period. The consolidation time effects were more significant in compression tests such that the peak strength increased with the consolidation period. The trend may be attributed to the creep-strain-rate effect during the anisotropic consolidation (see Table 1), which considerably expanded the elastic region on compression side.

The effect of consolidation period on the undrained shear (i.e., peak) strength, S_u, is examined in Figure10. Noting that the ratio of S_u to the consolidation stress, σ_{vc}, increased with the consolidation time, t normalized using the time to reach the end of primary consolidation, t_{3t}, the consolidation time effect may be expressed in the following;

$$\left(\frac{S_u}{\sigma_{vc}}\right)_{t_{total}} = m_c \ln\left(\frac{t_{total}}{t_{3t}}\right) + \left(\frac{S_u}{\sigma_{vc}}\right)_{t_{3t}} \tag{1}$$

where the m_c denotes a non-dimensional coefficient regarding the consolidation time effect on S_u/σ_{vc}.

The effects of consolidation period in the DSB test are shown in Figures 11, 12 and 13. It was observed that the S_u/σ_v increased with increasing consolidation period.

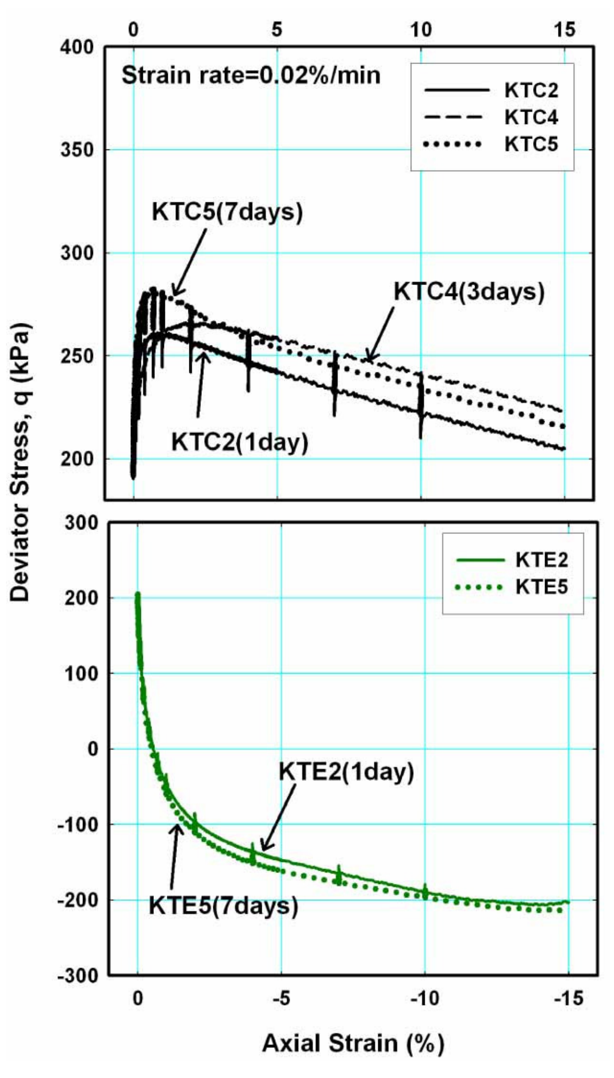

Figure 8 Stress-strain relationship of a series of triaxial tests using different consolidation times.

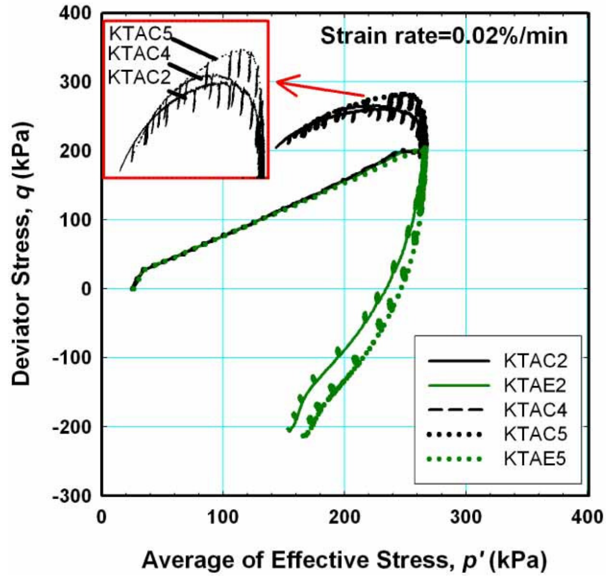

Figure 9 Undrained effective stress paths of a series of triaxial tests using different consolidation periods.

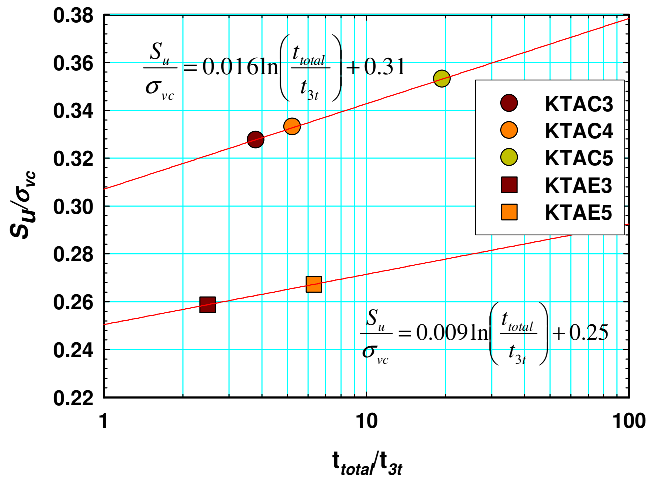

Figure 10 Effects of consolidation time on su/σvc in a series of triaxial tests

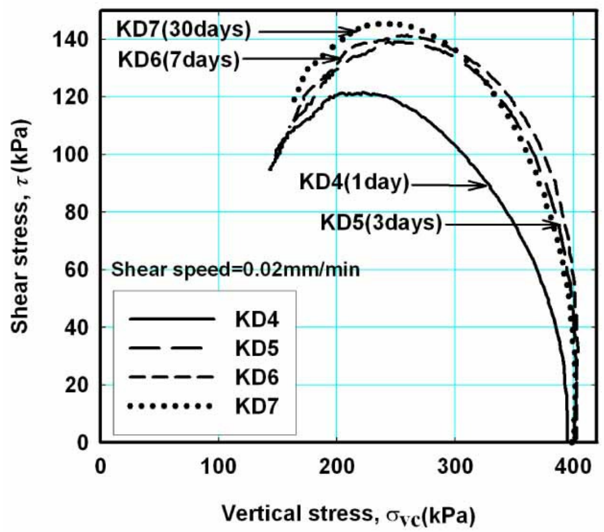

(a) τ-σvc relationship

Figure 11 Results of constant-volume DSB tests using different consolidation time.

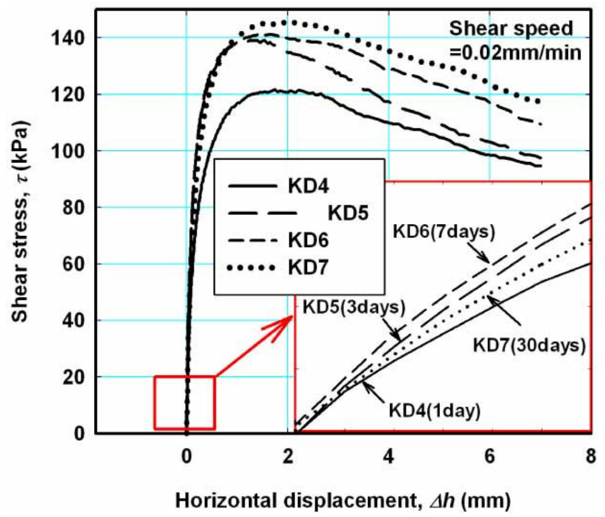

(b) τ-Δh relationship

Figure 12 Results of constant-volume DSB tests using different consolidation time.

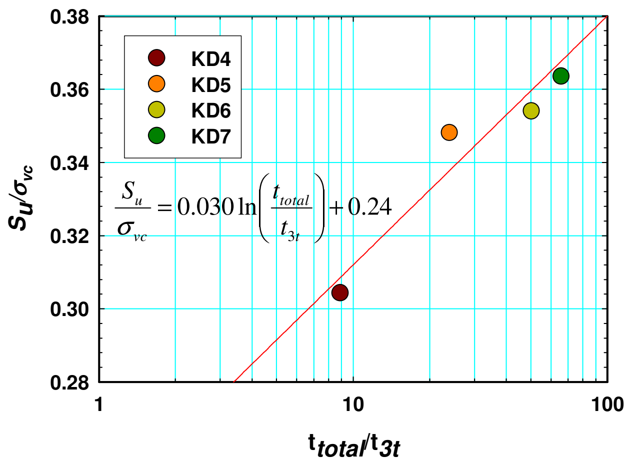

Figure 13 Effects of consolidation time on su/σvc in a series of constant-volume DSB test

4.2 Shear rate effects

Figures 14 and 15 show the results of a series of triaxial compression and extension tests using different, but fixed, axial strain rate. Similar results in DSB test are shown in Figure 16. As seen in Figure17, the S_u/σ_v increases with increasing strain rate (or shear displacement rate). Thus, based on the regression analysis using the date from experimental results, the following equation is determined to be the best fit:

$$\left(\frac{S_u}{\sigma_{vc}}\right)_{Vr} = m_r \ln(V_r) + \left(\frac{S_u}{\sigma_{vc}}\right)_{V_r=1} \tag{2}$$

where V_r represents the ratio of the current axial strain rate in triaxial test or the current shear displacement rate in DSB test to the reference value of 1%/min or 1mm/min, respectively.

4.3 Isotach behaviour

As seen in Figures14 and 15, the axial strain rate was altered in steps between 0.02%/min and 1%/min in two triaxial tests (one in compression and the other in extension). Isotach behaviour was obvious in that the stress-strain relationship as well as the undrained effective stress path shifted swiftly to the relevant stress-strain and stress path curves when the strain rate was changed in steps at 0.02%/min, 0.1%/min and 1%/min respectively.

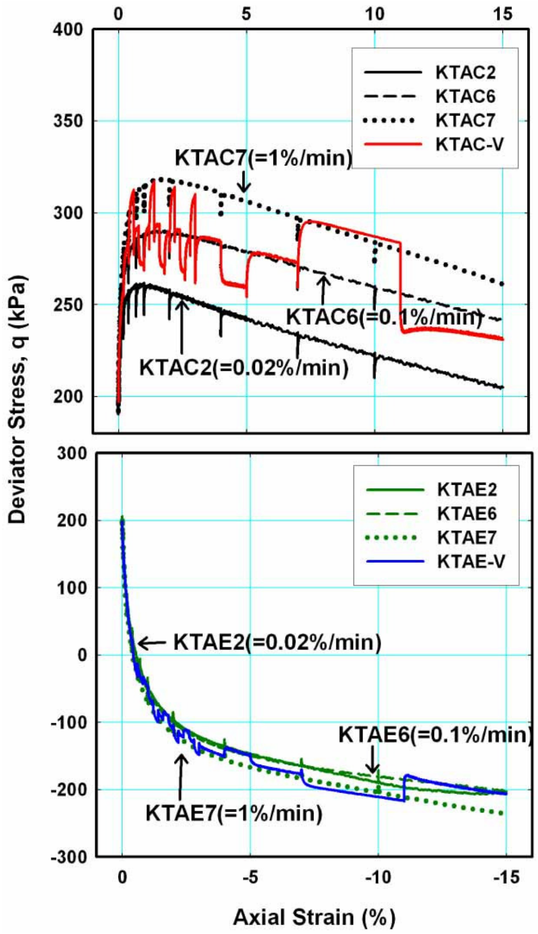

(a) anisotropically consolidated specimens

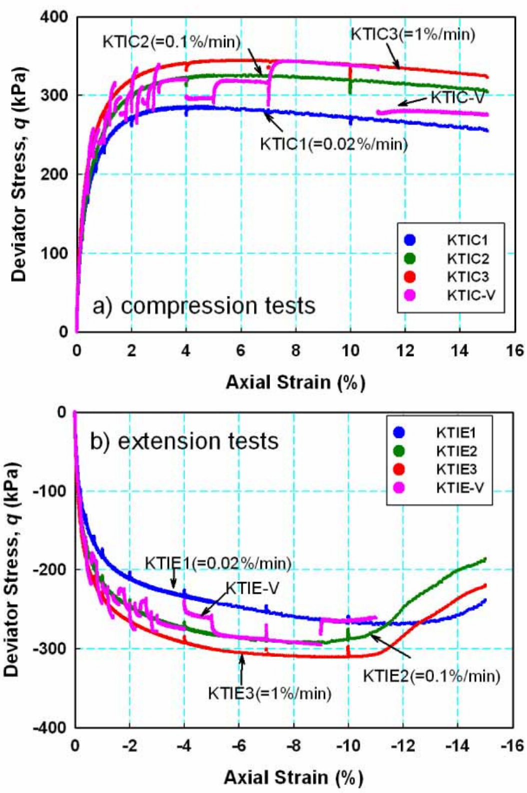

(b) isotropically consolidated specimens

Figure 14 Stress-strain relationship of a series of triaxial tests using different axial strain rates.

Such Isotach behaviour was also observed in a DSB test. As seen in Figure16, the shear stress-horizontal displacement relationship as well as the effective stress path shifted swiftly to the relevant curves when the shear rate was changed in steps at 0.02mm/min, 0.1mm/min and 1mm/min respectively. Figure 17 shows the effect of shear speed.

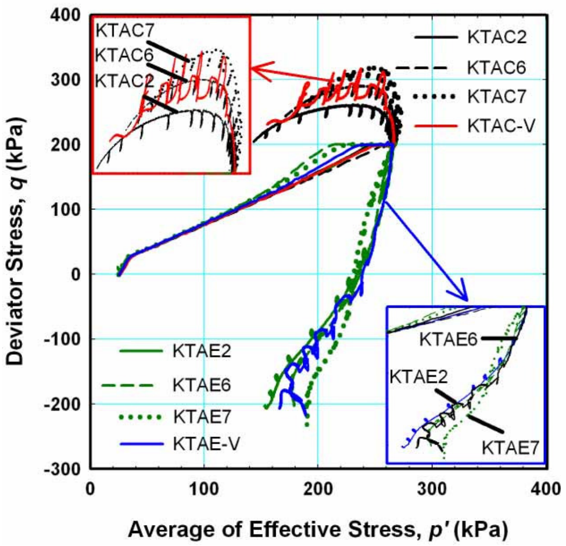

(a) anisotropically consolidated specimens

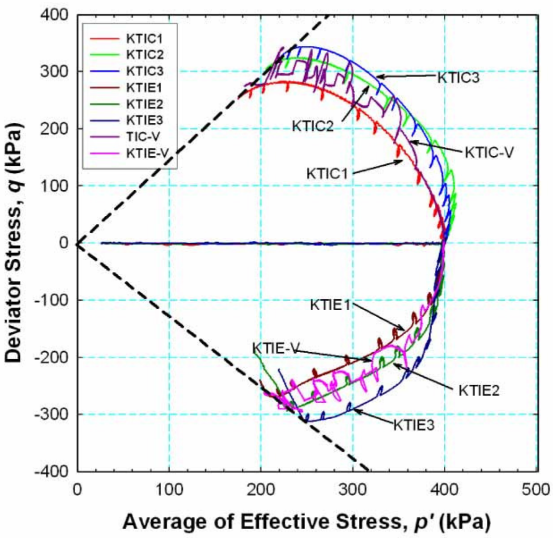

(b) isotropically consolidated specimens

Figure 15 Undrained effective stress paths of a series of triaxial tests using different axial strain rates.

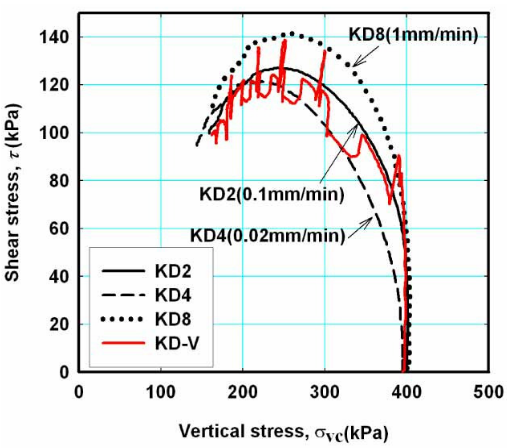

(a) τ-σ_{vc} relationship

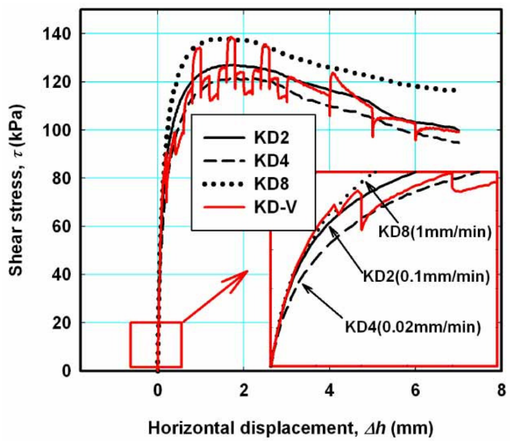

(b) τ-Δh relationship

Figure 16 Results of constant-volume DSB tests using different shear speeds.

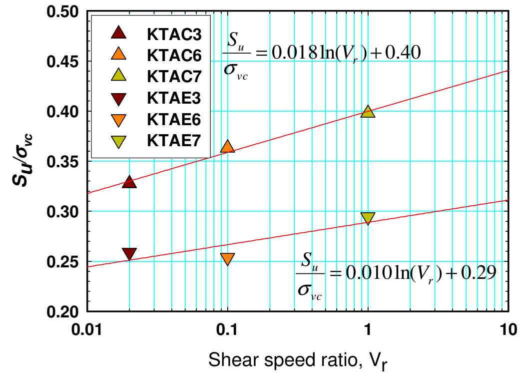

a) Triaxial test(anisotropically consolidated)

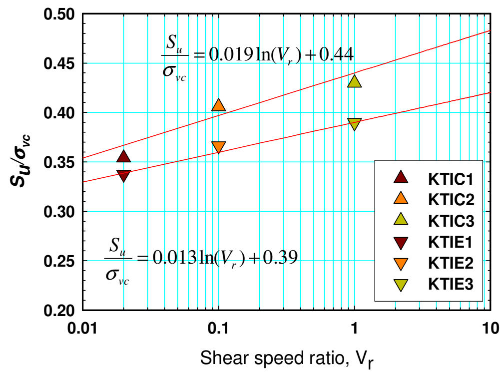

b) Triaxial test(anisotropically consolidated)

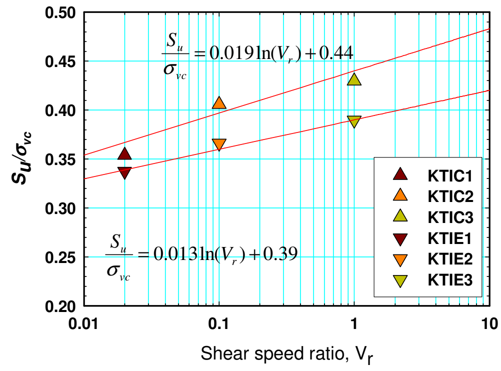

c) DSB test

Figure 17 Effects of shear speed on s_u/σ_{vc}; a) triaxial test(anisotropically consolidated), b) triaxial test(isotropically consolidated) and c) direct shear box test.

4.4 Comparison of undrained shear strength from different tests

A comparison of S_u/σ_{vc} among triaxial compression and extension tests, direct shear test and unconfined compression test is shown in Figure18. In this figure, the results of other tests, i.e., the unconfined compression test using very fresh samples from check boring and the triaxial compression and extension tests on isotropically consolidated samples are also shown for comparison.

When the samples were consolidated to a common 3t, the S_u/σ_{vc} value was larger in the order of triaxial compression, DSB and triaxial extension tests. The S_u/σ_{vc} value of 0.35 from unconfined compression test using fresh samples from check boring provided nearly the average of the S_u/σ_{vc} of these three tests, noting that the S_u/σ_{vc} of 0.35 was employed as the design value for constructing the sea-wall structure. Conversely, the S_u/σ_{vc} from unconfined compression test using old samples was about 0.22 on average, suggesting a considerable reduction of soil suction during transportation and storage.

As stated earlier, the S_u/σ_{vc} increased considerably as the shear rate as well as the consolidation period increased.

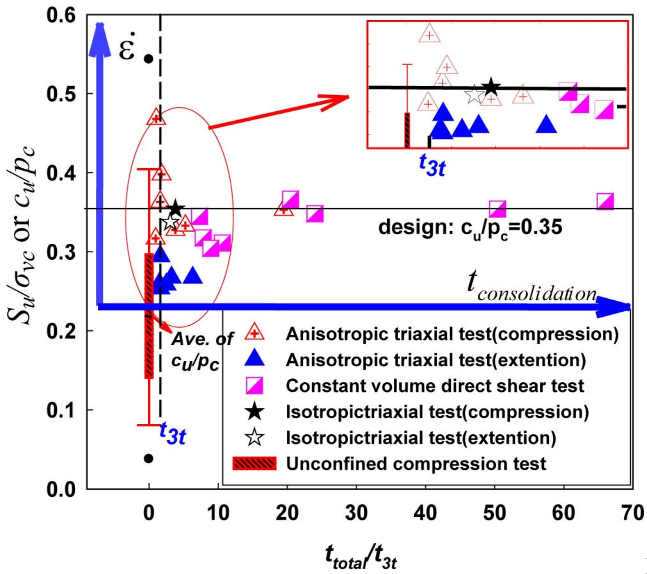

F

Figure 18 Comparison of undrained shear strength from different tests

5. SIMULATION OF UNDRAINED STRESS-STRAIN RELATIONSHIP

The results of a series of triaxial compression and extension tests are shown in Figure14 (a), in which the relationship between the deviator stress $q=\sigma_1-\sigma_3$ and the axial strain,ε, is plotted. The undrained effective stress paths in a plot of q versus the mean effective stress, $p'=(\sigma_1'+2\sigma_3')/3$, are shown in Figure15 (a). The samples were all consolidated anisotropically by maintaining the principal stress ratio K ($=\sigma'_3/\sigma'_1$) fixed at 0.5. On reaching the prescribed vertical consolidation stress of 400 kPa, the samples were subjected to undrained shear by using different axial strain rate. In tests KTAC-V and KTAE-V, the axial strain rate was altered in steps between 0.02%/min and 1%/min (for details, see Jung et al, 2008). It should be stated that the stress-strain response exhibited a type of Isotach behaviour; i.e., the current q was uniquely related to the current axial strain as well as the axial strain rate. Similar results of isotropically consolidated samples using K=1.0 are shown in Figures 14 (b) and 15 (b). In all the tests, cyclic loadings by using an axial strain amplitude of 0.005% were imposed at several stages, by which the variation of elastic stiffness during the undrained shear was examined, A basic equation for describing the stress-strain relationship may be expressed in the following form;

$$q = (q_{\max})_0 \cdot f(x) \cdot \left(\frac{\dot{\varepsilon}^{ir}}{\dot{\varepsilon}^{ir}_0} \right)^b \tag{3}$$

where

$\dot{\varepsilon}^{ir}$: the current irrecoverable strain rate,
q_{max} : strength at peak,
$f(x)$: shape function, and
b : an exponent.

The subscript "zero" means the reference values applicable to q_{max} and $\dot{\varepsilon}^{ir}$. An increment of irrecoverable strain due to Δq can be obtained using

$$\Delta\varepsilon = \Delta\varepsilon^e + \Delta\varepsilon^{ir} \tag{4}$$

Conversely, an increment of elastic strain, $\Delta\varepsilon^e$, was obtained from the elastic Young's modulus, E_e, in a manner that

$$\Delta\varepsilon^e = \frac{\Delta q}{E_e} \tag{5}$$

Figure 19 shows an example how $\Delta\varepsilon^e$ was obtained from the stress-strain relationship associated with the load-unload cycles. The variation of E_e with strain is shown in Figure 20, in which the results of three monotonic loading tests on the anisotropically consolidated samples, each using a fixed axial strain rate are plotted, together with the fitted curves. Note that the E_e decreased gradually with axial strain in all the tests. It should be mentioned that the accumulated ε^{ir} was obtained by integrating $\Delta\varepsilon^{ir}$ along the q-ε curve.

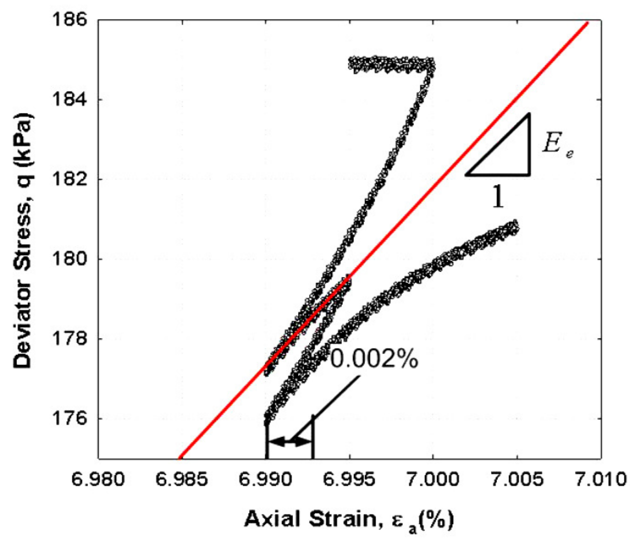

Figure 19 An example for the measurement of E_e

The shape function $f(x)$ is defined in terms of $x=\varepsilon^{ir}/\varepsilon_f$ where ε_f denotes the axial strain of 15% at the end of undrained shear. The $f(x)$ is shown in Figures 21 and 22 in which the increase of q from the value at the start of undrained shear, Δq, divided by the initial mean effective stress, p'_0, is plotted against x for anisotropically and isotropically consolidated specimens respectively.

The function takes the form of

$$f(x) = \alpha \exp\left[-0.5\left(\frac{\ln\left(\frac{x}{\chi}\right)}{\beta}\right)^2\right] \tag{6}$$

where the symbols α, β and χ are fitting parameters. These parameters indicated in Figures 21 and 22 were determined after iteration process of fitting the observed data.

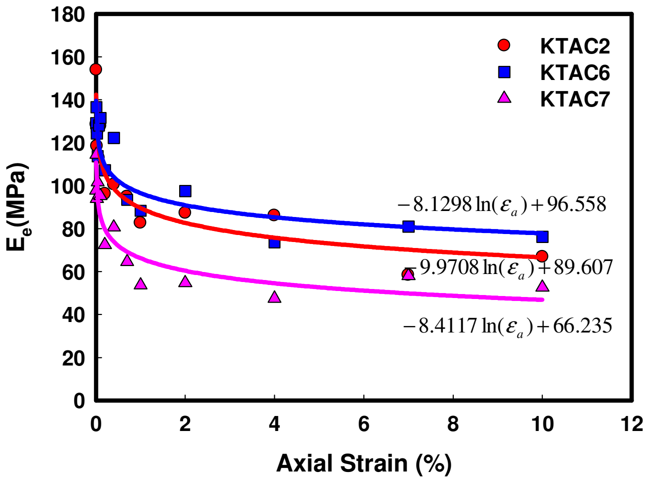

Figure 20 Relationship between Ee and axial strain for anisotropically consolidated specimens.

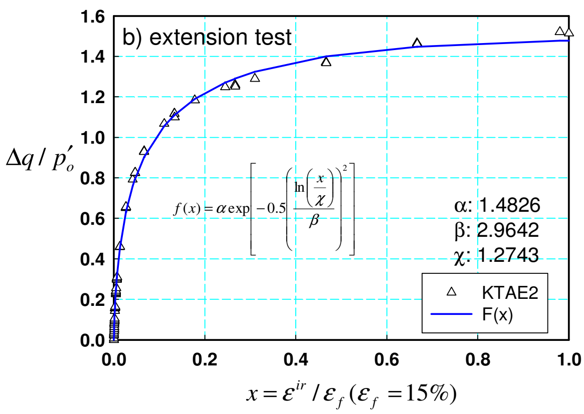

Figure 21 Shape function in the isotach model proposed (anisotropically consolidated specimens).

It was found that the exponent *b* in Eq (3) is not constant, but it varies with *x*, and the variation pattern in compression tests was different from that in extension tests on isotropically consolidated specimens. Two types of fitting function were employed for B(*x*), these are;

$$B(x) = \alpha e^{-\beta x} + \chi e^{-\delta x} + h \tag{7.a}$$

$$B(x) = \alpha \exp\left[-0.5\left(\frac{\ln\left(\frac{x}{\chi}\right)}{\beta}\right)^2\right] \tag{7.b}$$

The results of fitting are shown in Figures 23 and 24, for anisotropically and isotropically consolidated samples, respectively. Accordingly, the Isotach model proposed in this paper is given by

$$q = p'_0 \cdot f(x) \cdot \left(\frac{\dot{\varepsilon}^{ir}}{\dot{\varepsilon}^{ir}_0}\right)^{B(x)} \tag{8}$$

$$q = p'_0 \cdot f(x) \cdot A(\dot{\varepsilon}^{ir})^{B(x)} \tag{9}$$

The results of simulation are shown in Figures 25 and 26, in which the behaviour of an anisotropically consolidated specimen subjected to step-changes of axial strain rate was examined over the full and small strain ranges, respectively. Similar examination was made for the behaviour of an isotropically consolidated specimen (Figures 27 and 28). It is successfully demonstrated that the Isotach behaviour for the stress-strain relationship over a wide strain range from 0.001% to 15% was well simulated by using the proposed model.

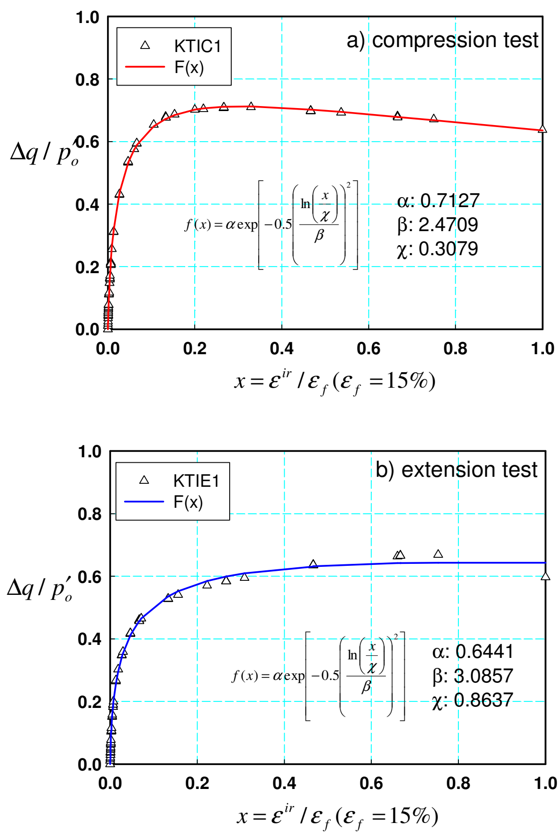

Figure 22 Shape function in the isotach model proposed (isotropically consolidated specimens).

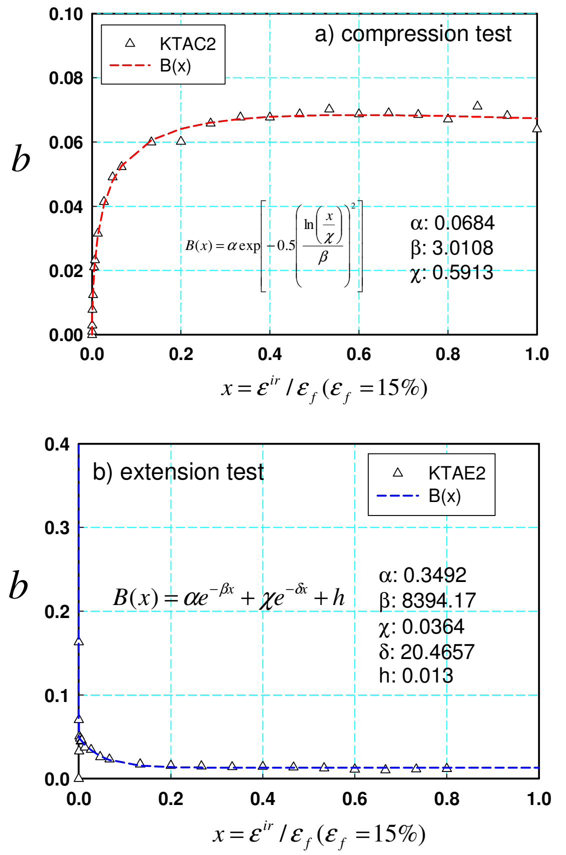

Figure 23 Exponent B(x) in the Isotach model proposed (anisotropically consolidated specimens).

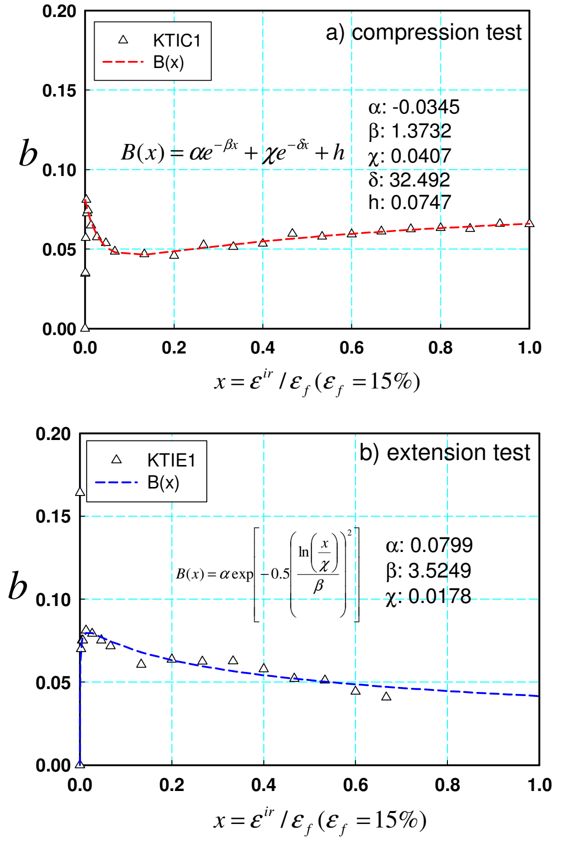

Figure 24 Exponent B(x) in the Isotach model proposed (isotropically consolidated specimens).

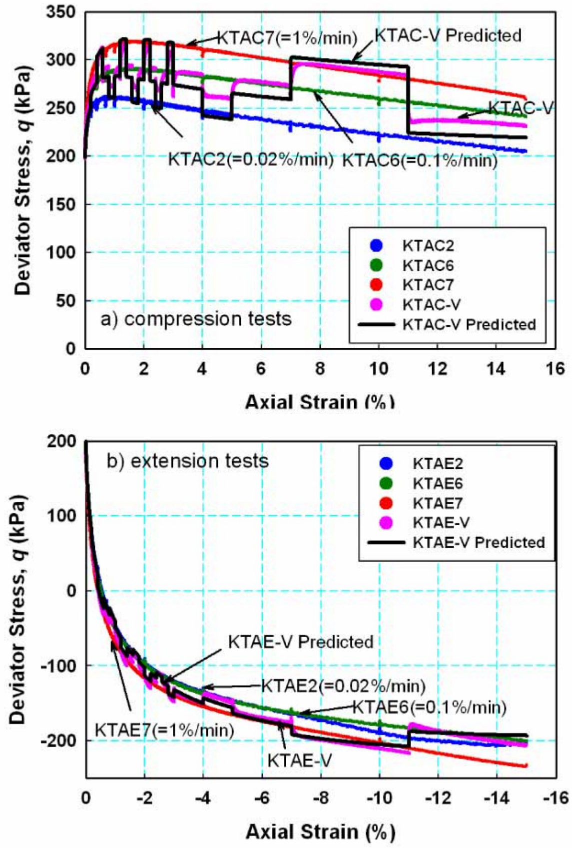

Figure 25 Predicted versus measured relationship between deviator stress and axial strain (full range of ε for anisotropically consolidated specimens).

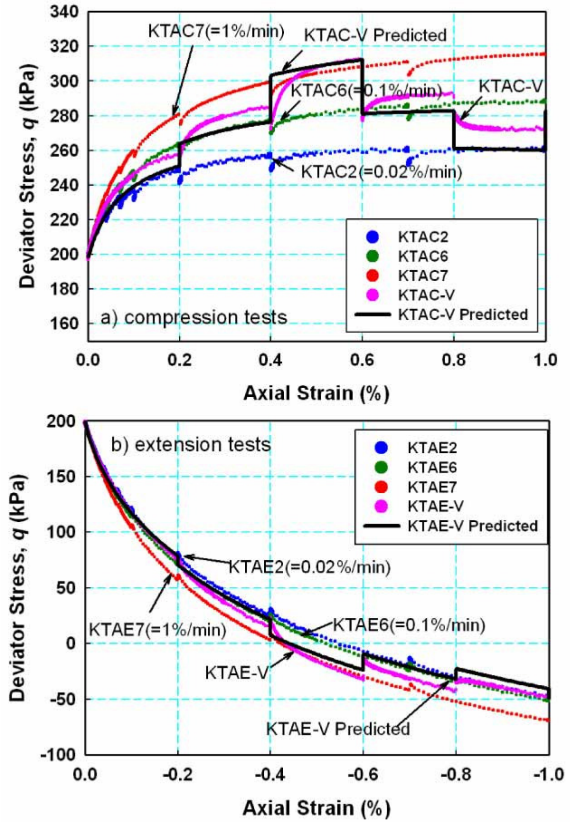

Figure 26 Predicted versus measured relationship between deviator stress and axial strain ($\varepsilon \leq 1\%$ for anisotropically consolidated specimens).

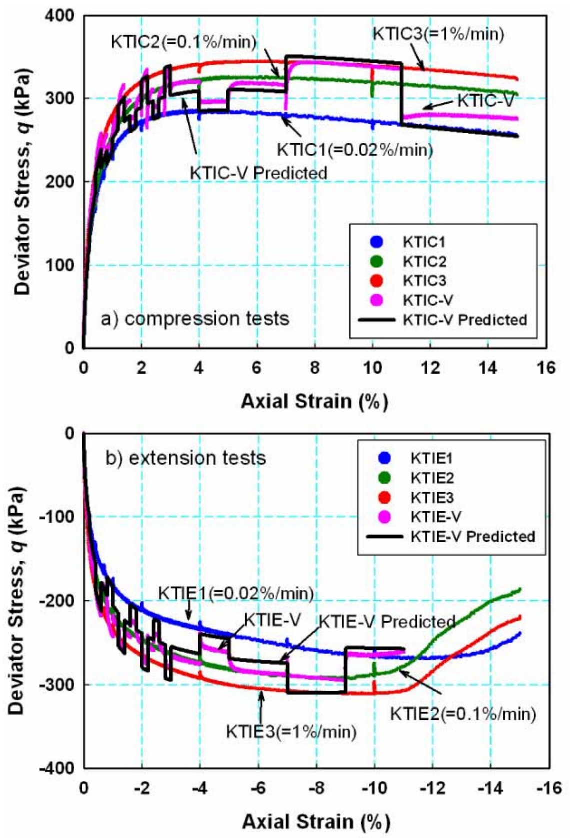

Figure 27 Predicted versus measured relationship between deviator stress and axial stain (full range of ε for isotropically consolidated specimens).

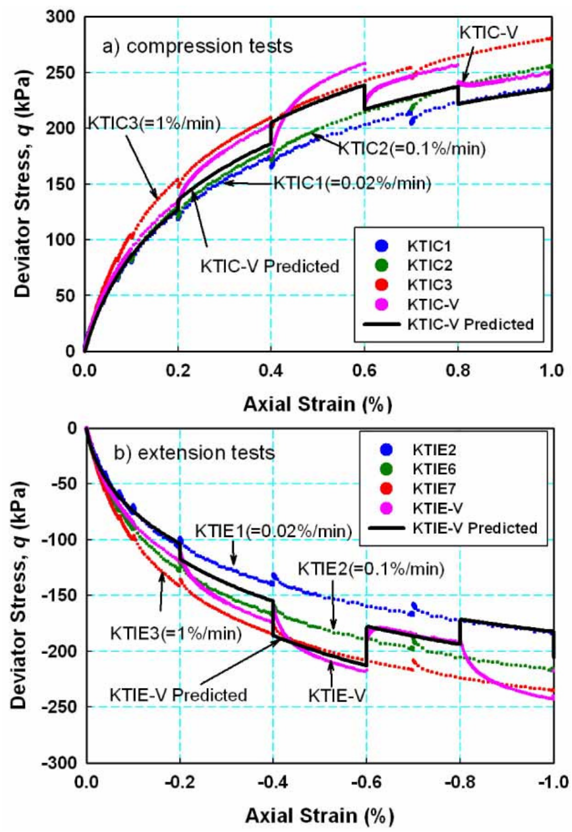

Figure 28 Predicted versus measured relationship between deviator stress and axial stain ($\varepsilon \leq 1\%$ for isotropically consolidated specimens)

6. PREDICTION OF DRAINED CREEP UNDER COSTANT VERTICAL STRESS

The results of a series of triaxial compression and extension tests are shown in Figure 14 (a), in which the relationship between the deviator stress $q = \sigma_1$-σ_3 and the axial strain,ε, is plotted.
Eq.(9) can be expressed in the following form;

$$\ln q = \ln p_0' + \ln f(x) + B(x)\ln A(\dot{\varepsilon}^{ir}) \tag{10}$$

Accordingly, Δq is given by

$$\Delta q = \left(\frac{\partial q}{\partial \varepsilon^{ir}} d\varepsilon^{ir} + \frac{\partial q}{\partial \dot{\varepsilon}^{ir}} d\dot{\varepsilon}^{ir} \right) \tag{11}$$

$$= \frac{1}{q} \left(\begin{array}{l} \dfrac{1}{\varepsilon_f} \dfrac{df(x)/dx}{f(x)} d\varepsilon^{ir} \\ + \dfrac{1}{\varepsilon_f} \dfrac{\partial B(x)}{\partial x} \ln A(\dot{\varepsilon}^{ir}) d\varepsilon^{ir} \\ + \dfrac{B(x)}{\dot{\varepsilon}^{ir}} d\dot{\varepsilon}^{ir} \end{array} \right)$$

When considering drained creep with Δq=0, we obtain;

$$d\varepsilon^{ir} = -c_r \frac{d\dot{\varepsilon}^{ir}}{\dot{\varepsilon}^{ir}} \tag{12}$$

$$c_r = \frac{B(x) \cdot \varepsilon_f}{\left(\dfrac{df(x)/dx}{f(x)} + \dfrac{\partial B(x)}{\partial x} \ln A(\dot{\varepsilon}^{ir}) \right)} \tag{13}$$

where c_r represents the coefficient of creep.

Provided that c_r is unaffected by the strain rate, the c_r increases monotonically with strain. At the commencement of creep at t=0, the initial strain rate $\dot{\varepsilon}_{ini}^{ir}$ an be readily measured. Therefore, the creep strain with the elapsed time, Δt, is given by

$$\Delta \varepsilon^{ir} = c_r \ln\left(\frac{\Delta t \cdot \dot{\varepsilon}_{ini}^{ir}}{c_r} + 1 \right) \tag{14}$$

The development of creep strain with time is shown in Figure 29, in which the data refers to the creep strain development at consolidation stage of a triaxial sample under the prescribed vertical consolidation stress. The prediction using Eq.(14) seems satisfactory as validated over a period of one day.

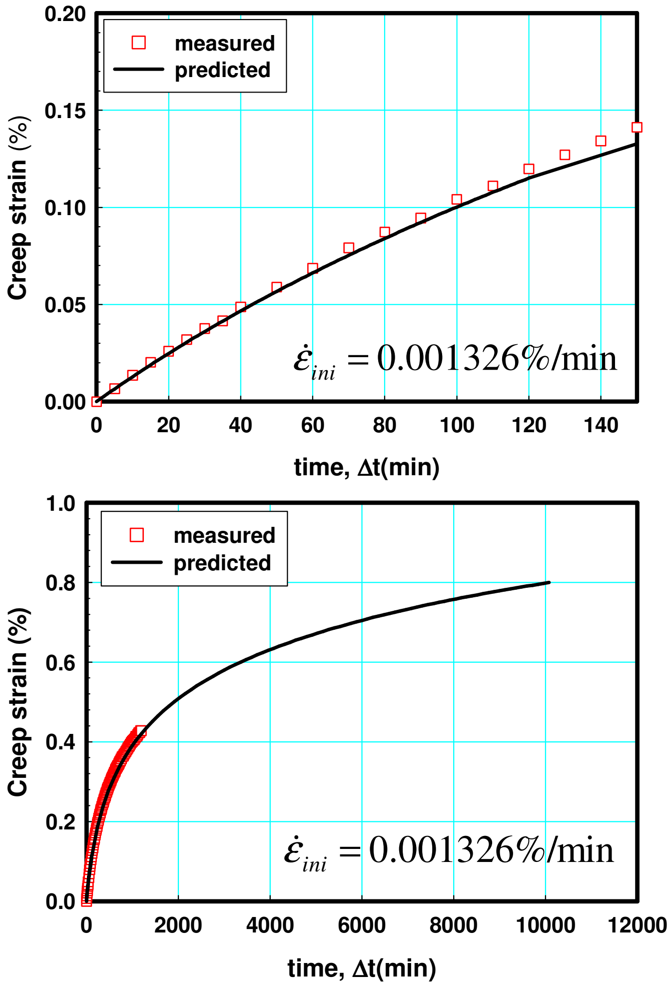

Figure 29. Prediction of drained creep behaviour.

7. CONCLUSION

Rate as well as time effects were significant for undrained shear behaviour of Holocene clay at Kobe airport. The S_u/σ_{vc} value increased with the shear rate as well as the consolidation period as examined in both triaxial and DSB tests. Isotach properties were also observed in a manner that the stress-strain relationship as well as the undrained stress path was uniquely related to the current shear rate. When the samples were consolidated to a common 3t, the S_u/σ_{vc} value was larger in the order of triaxial compression, DSB and triaxial extension tests. The S_u/σ_{vc} value from unconfined compression test using fresh samples from check boring provided nearly the average of the S_u/σ_{vc} of these three tests.

It is concluded that the Holocene clay exhibits Isotach behaviour based on the results of triaxial compression and extension tests. Such a behaviour, which is verified by the experimental results, was successfully simulated by the model given in Eq.(8). The development of drained creep strain with time under the condition of Δq=0 was also successfully predicted by using Eq.(14).

8. REFERENCES

Bjerrum, L., (1972) "Embankments on soft ground", Proceedings of Int. ASCE Specialty Conf. on Performances of Earth and Earth-Supported Structures, Vol. 2, Lafayette, Indiana, pp1-54.

Di Benedetto, H. and Tatsuoka, F., (1997) "Small strain behavior of geomaterials: Modeling of strain rate effects", Soils and Foundations, Vol.37, No.2, pp127-138.

Fujiwara, T., Shibuya, S., Takayama, K., Kawaguchi, T. and Hasegawa, N., (2008) "Strain-rate dependent yielding of Pleistocene Clay subjected to one-dimensional compression", Proc. of 11th ISC'3, Taipei, pp135-145

Graham, J., Crooks, J. H. A. and Bell, A.L.(1983) "Time effects on the stress-strain behaviour of natural soft clay", Géotechnique, Vol.33, No.3, pp327-340.

Hanzawa, H. and Kishida, T., (1981) "Fundamental considerations on undrained strength characteristics of alluvial marine clays", Soils and Foundations, Vol. 21, No. 1, pp39-50.

Japanese Geotechnical Society (JGS). (1979) Soil test method, 2nd revised edition, , pp495-530 (in Japanese).

Oshima, A., Takada, N. and Mikasa, M., (1991) "Strength anisotropy of clay in slope stability", Centrifuge91, Balkema, pp591-598.

Shibuya, S., Mitachi, T. and Tamate, S., (1997) "Interpretation of direct shear box testing of sand as quasi-simple shear", Geotechnique, Vol.47, No.4, pp769-790.

Shibuya, S., Mitachi, T., Tanaka, H., Kawaguchi, T. and Lee, I.M.,(2001) "Measurement and application of quasi-elastic properties in geotechnical site characterization", Theme Lecture, Proc. of 11th Asian Regional Conference on SMGE, Seoul, Balkema, Vol. 2, , pp639-710.

Shibuya, S., Koseki, J. and Kawaguchi, T.(2005) "Recent developments in deformation and strength testing of geomaterials", Keynote Lecture, Deformation Characteristics of Geomaterials-Recent Investigations and Prospects (Di Benedetto H. et al edns), Taylor Francis Group London, , pp3-28.

Šuklie, L.,(1969) "Rheological Aspects of Soil Mechanics", Wiley-Interscience,.

Tatsuoka, F.(1999) "Isotach behaviour of geomaterials and its modeling", Proc. Second Int. Conf. on Pre-Failure Deformation Characteristics of Geomaterials, IS Torino '99, Balkema, Vol.1, , pp491-499.

Vaid, Y.P. and Campanella, R.G.,(1977) "Time dependent behaviour of undisturbed clay", Journal of the Geotechnical Engineering Div., Proc. of ASCE, Vol.103, No.7, , pp693-709.